

Quarkonium Spectroscopy and Perturbative QCD: A New Perspective*

Y. Sumino

Department of Physics, Tohoku University
Sendai, 980-8578 Japan

Abstract

We report new aspects of the recent theoretical progress in heavy quarkonium physics. (1) Contrary to wide beliefs, the gross structure of the bottomonium spectrum is described well by the non-relativistic boundstate theory based on perturbative QCD. (2) This leads to a new physical picture of the bottomonium states: the boundstate mass is composed mainly of the self-energies of b and \bar{b} accumulated inside the boundstate. (3) A connection to the conventional phenomenological potential-model approaches is provided.

*Talk given at “Accelerator and Particle Physics Institute (APPI 2001)”, Morioka, Japan, Feb. 20–22, 2001.

1 Introduction

In this paper we review the results of the recent studies on the spectra of heavy quarkonia (bottomonium, charmonium and B_c states) [1, 2]. We focus mainly on the bottomonium spectrum below; the results of the charmonium and B_c spectra will be summarized at the end of the paper.

For over 20 years, major theoretical approaches to the charmonium and bottomonium spectroscopy have been those based on various phenomenological potential models. In each of the models a non-relativistic Hamiltonian,

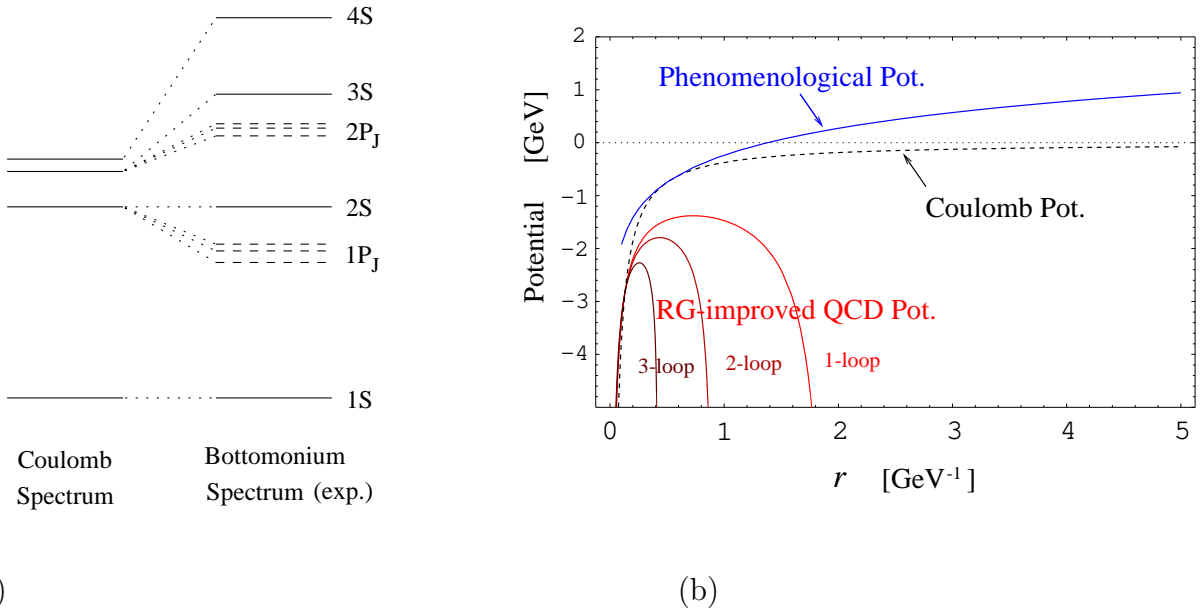
$$\hat{H} = \frac{\vec{p}^2}{2m_r} + V_{\text{pheno}}(r), \quad (1)$$

is assumed and a phenomenological potential $V_{\text{pheno}}(r)$ is determined such that the observed quarkonium spectra (and some other physical observables) are reproduced, starting from a simple ansatz for the form of the potential. The determined potentials in all models have more or less similar slopes in the range $0.5 \text{ GeV}^{-1} \lesssim r \lesssim 5 \text{ GeV}^{-1}$, which may be represented by a logarithmic potential $\propto \log r + \text{const}$. These phenomenological-model approaches have successfully elucidated nature of the quarkonium systems, such as their leptonic widths and transitions among different levels, besides reproducing the energy levels. See e.g. Ref.[3] for a most recent analysis based on the potential models. An apparent deficit of these approaches is, however, a difficulty in relating phenomenological parameters to the fundamental parameters of QCD.

The reason why people had to resort to phenomenological models is because the theory of non-relativistic boundstates, which has been successful in describing the spectra of the QED boundstates, failed to reproduce the charmonium and bottomonium spectra in QCD. Within this theory, the quarkonium states in the leading approximation are described by the Hamiltonian of non-relativistic quantum mechanics with a Coulomb potential

$$V_C(r) = -C_F \frac{\alpha_S}{r}. \quad (2)$$

It stems from one gluon exchange between the quark and antiquark, where $C_F = 4/3$ is a color factor. Compare the observed bottomonium spectrum and the Coulomb spectrum shown in Fig. 1(a). In the Coulomb spectrum, the level spacing between consecutive nS states decreases rapidly as $1/n^2$. On the other hand in the bottomonium spectrum the level spacing appears roughly constant; furthermore, the separations between the S and P states as well as the fine splittings among nP_J states are sizable. Thus, the level structures look qualitatively very different. Including higher order corrections, the Coulomb potential changes to the QCD potential, which is given roughly by replacing α_S in the numerator of Eq. (2) with the running coupling constant evaluated at scale $1/r$, i.e. $\alpha_S(\mu = 1/r)$. Accordingly the QCD potential is bent downwards at long distances as compared to the Coulomb potential. As can be seen in Fig. 1(b), the QCD potential becomes singular at a fairly short distance. At $r \gtrsim 0.2 \text{ GeV}^{-1}$, the QCD



(a) (b)

Figure 1: (a) A comparison of the Coulomb spectrum and the observed bottomonium spectrum. The parameters m_b and α_S of the Coulomb spectrum are adjusted to reproduce the observed 1S and 2S levels. (b) A comparison of the renormalization-group-improved QCD potential, the Coulomb potential and a typical phenomenological potential.

potential is poorly convergent as the higher order corrections are included. There seems to be no chance that it explains the phenomenologically determined potentials, which deviate from the Coulomb potential in the upward (i.e. opposite) direction. The large discrepancy of the QCD potential and phenomenological potentials, as well as the poor convergence of the QCD potential, have been thought as indications of large non-perturbative effects inherent in the heavy quarkonium systems. In fact the difference between a typical phenomenological potential and the Coulomb potential tends to be a linearly rising potential at distances $r \gtrsim 1 \text{ GeV}^{-1}$, suggesting confinement of quarks.

During the last few years, the theory of non-relativistic QCD boundstates has developed remarkably. There were two important developments: (1) The complete next-to-next-to-leading order corrections to the energy levels have been computed [4, 5, 6, 7, 8]. Also, some of the (non-trivial) next-to-next-to-next-to-leading order corrections have been calculated [9, 10, 11]. (2) The renormalon cancellation in the energy levels was discovered [12, 13]. The upshot is that convergence of the perturbative expansions of the energy levels improves drastically if we express the levels in terms of the $\overline{\text{MS}}$ mass instead of the pole mass of a quark. These theoretical developments enabled accurate perturbative computations of the quarkonium energy levels. Let us demonstrate the improvement of convergence for the $\Upsilon(1S)$ and $\Upsilon(2S)$ states:

- $\Upsilon(1S)$: For $\mu = 2.49$ GeV, $\alpha_S(\mu) = 0.274$, $m_b^{\overline{\text{MS}}}(m_b^{\overline{\text{MS}}}) = 4.20$ GeV/ $m_{b,\text{pole}} = 4.97$ GeV,

$$M_{\Upsilon(1S)} = 9.94 - 0.17 - 0.20 - 0.30 \text{ GeV} \quad (\text{Pole-mass scheme}) \quad (3)$$

$$= 8.41 + 0.84 + 0.20 + 0.013 \text{ GeV} \quad (\overline{\text{MS}}\text{-scheme}). \quad (4)$$
- $\Upsilon(2S)$: For $\mu = 1.09$ GeV, $\alpha_S(\mu) = 0.433$, $m_b^{\overline{\text{MS}}}(m_b^{\overline{\text{MS}}}) = 4.20$ GeV/ $m_{b,\text{pole}} = 4.97$ GeV,

$$M_{\Upsilon(2S)} = 9.94 - 0.10 - 0.19 - 0.45 \text{ GeV} \quad (\text{Pole-mass scheme}) \quad (5)$$

$$= 8.41 + 1.46 + 0.093 + 0.009 \text{ GeV} \quad (\overline{\text{MS}}\text{-scheme}). \quad (6)$$

As can be seen, when the pole mass is used the series are not converging, whereas the series show healthy convergent behaviors when the $\overline{\text{MS}}$ mass is used. As important applications of these developments up to date, the theory enabled precise determinations of the $\overline{\text{MS}}$ -mass of the bottom quark [5, 14, 6, 15] and (in the future) of the top quark [16] from (mainly) the energy levels of the lowest-lying states. The main uncertainty comes, in the bottomonium case, from the (essentially) unknown non-perturbative contributions. These are generally claimed to be around 100 MeV and ultimately set the precision of the prediction.

Based on the above theoretical developments we analyze the consistency between the whole level structure of the quarkonium as predicted by the boundstate theory (perturbative QCD) and that of the experimental data. Now that we can make accurate predictions, we can extract upper bounds on the non-perturbative contributions to the energy levels by comparing the perturbative predictions, at the current best accuracy, with the experimental data. It turns out that non-perturbative effects should be much smaller than what have been believed conventionally.

The paper is organized as follows. In Sec. 2 we review briefly the necessary theoretical framework. We analyze the bottomonium spectrum numerically in Sec. 3 and estimate the errors of the theoretical predictions in Sec. 4. We interpret the result and provide a new physical picture of the bottomonium states in Sec. 5. Then we discuss a connection between our approach and the phenomenological potential-model approaches in Sec. 6. We draw conclusions in Sec. 7.

2 Theoretical Framework

2.1 $1/c$ expansion

We state briefly the theoretical framework used in contemporary calculations of the spectrum of heavy quarkonia. The problem is reduced to a quantum mechanical one as follows. We first compute the quark-antiquark (off-shell) scattering amplitude in ordinary perturbative QCD. We then determine a quantum mechanical Hamiltonian such that the quark-antiquark scattering

amplitude computed within quantum mechanics matches the former amplitude order by order in expansion in $1/c$ (inverse of the speed of light):

$$\hat{H} = \hat{H}_0 + \frac{1}{c} \hat{H}_1 + \frac{1}{c^2} \hat{H}_2 + \dots \quad (7)$$

The expansion is a double expansion in $\alpha_S = g_S^2/(4\pi\hbar c)$ and $\beta = v/c$. Then we solve the non-relativistic Schrödinger equation

$$\hat{H} \psi_n(r) = E_n \psi_n(r) \quad (8)$$

to determine the boundstate wave functions and energy spectrum, order by order in $1/c$ expansion. Provided the quark and antiquark inside the heavy quarkonium are non-relativistic, the expansion in $1/c$ leads to a reasonable systematic approximation.

It should be noted that this procedure parallels a more familiar procedure for the calculation of the masses of one-particle states. The matrix element of the above Hamiltonian $\langle \vec{p} | \hat{H} | \vec{p}' \rangle$ is, in the language of perturbative QCD, the sum of two-particle irreducible diagrams.* One may then compare Eq. (8) with e.g. the computation of the photon and Z boson masses by solving the eigenvalue equation

$$s\mathbf{1} - \begin{pmatrix} \Pi_{\gamma\gamma}(s) & \Pi_{\gamma Z}(s) \\ \Pi_{Z\gamma}(s) & \Pi_{ZZ}(s) \end{pmatrix} = 0,$$

where $\Pi_{ij}(s)$ represent the sums of one-particle irreducible diagrams [$\Pi_{ZZ}(s)$ includes $M_Z^{(\text{tree})}$].

Presently the Hamiltonian is known up to $\mathcal{O}(1/c^2)$ in the Coulomb gauge [5, 18]:

$$\hat{H}_0 = \frac{\vec{p}^2}{m} - C_F \frac{\alpha_S}{r}, \quad (9)$$

$$\hat{H}_1 = -C_F \frac{\alpha_S}{r} \cdot \left(\frac{\alpha_S}{4\pi} \right) \cdot \left\{ \beta_0 \log(\mu'^2 r^2) + a_1 \right\}, \quad (10)$$

$$\begin{aligned} \hat{H}_2 = & -\frac{\vec{p}^4}{4m^3} - C_F \frac{\alpha_S}{r} \cdot \left(\frac{\alpha_S}{4\pi} \right)^2 \cdot \left\{ \beta_0^2 [\log^2(\mu'^2 r^2) + \frac{\pi^2}{3}] + (\beta_1 + 2\beta_0 a_1) \log(\mu'^2 r^2) + a_2 \right\} \\ & + \frac{\pi C_F \alpha_S}{m^2} \delta^3(\vec{r}) + \frac{3C_F \alpha_S}{2m^2 r^3} \vec{L} \cdot \vec{S} - \frac{C_F \alpha_S}{2m^2 r} \left(\vec{p}^2 + \frac{1}{r^2} r_i r_j p_j p_i \right) - \frac{C_A C_F \alpha_S^2}{2m r^2} \\ & - \frac{C_F \alpha_S}{2m^2} \left\{ \frac{S^2}{r^3} - 3 \frac{(\vec{S} \cdot \vec{r})^2}{r^5} - \frac{4\pi}{3} (2S^2 - 3) \delta^3(\vec{r}) \right\}, \end{aligned} \quad (11)$$

where m denotes the pole mass of the quark; $\alpha_S \equiv \alpha_S(\mu)$; $C_F = 4/3$, $C_A = 3$ are color factors; $\mu' = \mu e^{\gamma_E}$. The lowest-order Hamiltonian \hat{H}_0 is nothing but that of two equal-mass particles interacting via the Coulomb potential.

* This is true with respect to the diagrams in the time-ordered (old-fashioned) perturbation theory [17].

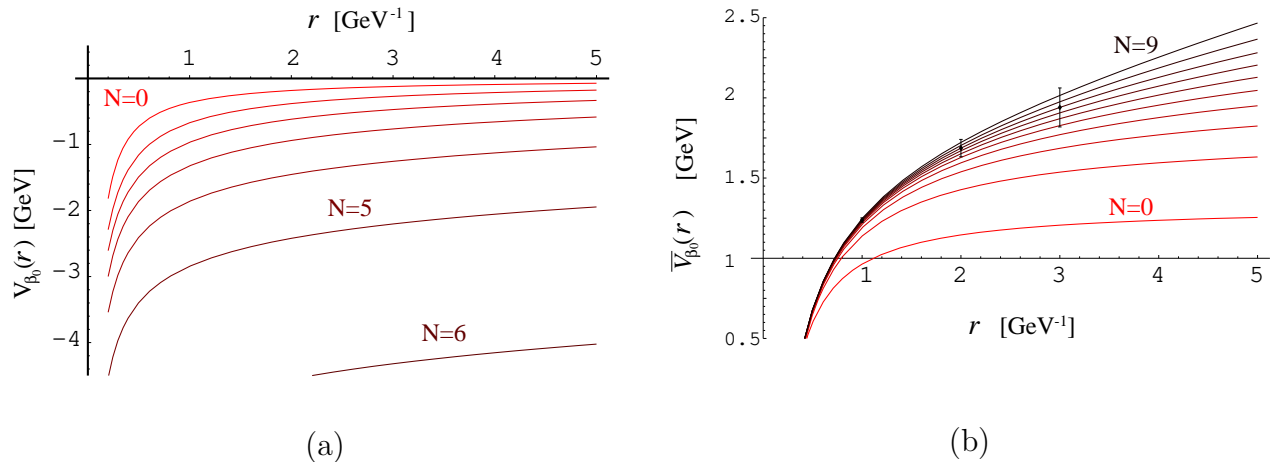


Figure 2: The QCD potential in the large- β_0 approximation truncated at $O(\alpha_S^{N+1})$ term. We set $\mu = 2.49$ GeV, $n_l = 4$ and $\alpha_S(\mu) = 0.273$ [corresponding to $\alpha_S^{(5)}(M_Z) = 0.1181$]. (a) Before subtraction of the leading renormalon. (b) After subtraction of the leading renormalon. These figures are taken from [2].

2.2 Renormalon cancellation

In addition to the first three terms $\hat{H}_0, \hat{H}_1, \hat{H}_2$ of the Hamiltonian, part of the higher order terms \hat{H}_n are known. Specifically, these are part of the static QCD potential $V_{\text{QCD}}(r)$. From their analysis, it has been known [19] that the series expansion of $V_{\text{QCD}}(r)$ in $\alpha_S(\mu)$ diverges rapidly at high orders, and that this results in an uncertainty of $V_{\text{QCD}}(r)$ of order Λ_{QCD} even within perturbative QCD. This problem is referred to as the renormalon problem. This is demonstrated in Fig. 2(a), where the QCD potential in the so-called “large- β_0 approximation” is shown up to the $(N+1)$ -th term, $\sum_{n=0}^N V_{\beta_0}^{(n)}(r)$, for $N = 0, 1, 2, \dots$ and $n_l = 4$. We see that the higher order corrections are indeed large and almost constant (independent of r).

It was found [12, 13] that the leading renormalons contained in the pole mass [20] and in the QCD potential [19] cancel in the total energy of a static quark-antiquark pair if the pole mass m_{pole} is expressed in terms of the $\overline{\text{MS}}$ mass:

$$E_{\text{tot}}(r) \equiv 2m_{\text{pole}} + V_{\text{QCD}}(r), \quad (12)$$

$$V_{\text{QCD}}(r) \simeq - \int \frac{d^3\vec{q}}{(2\pi)^3} e^{i\vec{q}\cdot\vec{r}} C_F \frac{4\pi\alpha_S(q)}{q^2}, \quad (13)$$

$$m_{\text{pole}} \simeq m_{\overline{\text{MS}}}(\mu) + \frac{1}{2} \int_{q<\mu} \frac{d^3\vec{q}}{(2\pi)^3} C_F \frac{4\pi\alpha_S(q)}{q^2}, \quad (14)$$

where $q = |\vec{q}|$. The above equations show that the potential $V_{\text{QCD}}(r)$ is essentially the Fourier transform of the Coulomb gluon propagator exchanged between quark and antiquark, and that the difference of m_{pole} and $m_{\overline{\text{MS}}}$ is essentially the infrared portion of the quark self-energy. The renormalon contributions originate from the infrared region, $q \sim \Lambda_{\text{QCD}}$, of the loop integrations,

where the running coupling constant $\alpha_S(q)$ becomes large. Namely the infrared gluons cause bad behaviors of the perturbation series at high orders. The signs of the renormalon contributions are opposite between $V_{\text{QCD}}(r)$ and m_{pole} because the color charges are opposite between quark and antiquark while the self-energy is proportional to the square of a same charge. Their magnitudes differ by a factor of two because both the quark and antiquark propagator poles contribute in the calculation of the potential whereas only one of the two contributes in the calculation of the self-energy. Expanding the Fourier factor $e^{i\vec{q}\cdot\vec{r}}$ in a Taylor series for small \vec{q} , the leading renormalon contributions cancel in $E_{\text{tot}}(r)$.

As a result of this cancellation, the series expansion of the total energy in $\alpha_S(\mu)$ converges better if we use the $\overline{\text{MS}}$ mass instead of the pole mass. In order to demonstrate the improvement of convergence, we show in Fig. 2(b) the QCD potential in the large- β_0 approximation [up to the $(N+1)$ -th term] after the leading renormalon is subtracted at each order of $\alpha_S(\mu)$. One sees that the series expansion of the potential has become much more convergent as compared to Fig. 2(a). Note that the higher-order corrections raise the potential at long distances after subtraction of the renormalon contribution. Some important aspects are:

- The pole mass of a quark is ill-defined beyond perturbation theory. It can be determined only when the quark can propagate an infinite distance. Generally accepted belief is that when quark and antiquark are separated beyond a distance $\sim \Lambda_{\text{QCD}}^{-1}$ the color flux is spanned between the two charges due to non-perturbative effects and the free quark picture is no longer valid. On the other hand, the total energy (or the mass) of a quarkonium, which is a color-singlet state, is physically meaningful. A color-singlet state can propagate for a long time and the notion of its mass is not limited by the hadronization scale.
- When the size of a color-singlet system is much smaller than $\Lambda_{\text{QCD}}^{-1}$, infrared gluons with wavelengths $\Lambda_{\text{QCD}}^{-1}$ cannot couple to color sources inside the system — such a picture is naturally described by the bare QCD Lagrangian. Hence, if we use $m_{\overline{\text{MS}}}$, which is more closely related to the bare mass than m_{pole} is, contributions from the infrared gluons vanish in $E_{\text{tot}}(r)$.

See e.g. [21] for an introductory review of the renormalons in the heavy quarkonium states.

3 Bottomonium Spectrum: A Numerical Analysis

In this section we examine the bottomonium spectra numerically [1]. According to the formalism explained in the previous section, the energy levels are computed analytically as functions of $\alpha_S(\mu)$, μ and $\overline{m}_b \equiv m_b^{\overline{\text{MS}}}(m_b^{\overline{\text{MS}}})$ (the b -quark $\overline{\text{MS}}$ mass renormalized at the $\overline{\text{MS}}$ -mass scale). The dependence on the scale μ arises from truncation of the series expansion at finite order. In this section we set the number of massless flavors as $n_l = 4$ and neglect the effects of the non-zero charm quark mass in the $b\bar{b}$ systems.

The algorithm of our calculations goes as follows.

1. We take the strong coupling constant with the present world average value as input,[†] $\alpha_S^{(5)}(M_Z) = 0.1181 \pm 0.0020$ [22].
2. The scale μ is fixed for each state X from the minimal sensitivity condition:

$$\left. \frac{d}{d\mu} E_X(\mu, \alpha_S(\mu), \overline{m}_b) \right|_{\mu=\mu_X} = 0. \quad (15)$$

3. We fix \overline{m}_b from the mass of the vector ground state:

$$E_{\Upsilon(1S)}(\mu_{1S}, \alpha_S(\mu_{1S}), \overline{m}_b) = E_{\Upsilon(1S)}^{exp} = 9.460 \text{ GeV}. \quad (16)$$

A comment regarding the scale determined by the scale-fixing prescription Eq. (15) is in order. We find that, for most of the bottomonium states, the convergence properties of the series become optimal at $\mu \simeq \mu_X$, and that the scale becomes close to the inverse of the physical size of the boundstate X . If the scale fixed by Eq. (15) evidently does not fulfill these conditions, then the theoretical predictions obtained in this way will be considered *unreliable*. We will show that this typically happens for the higher levels, where the coupling constant becomes bigger than one.

The b -quark $\overline{\text{MS}}$ mass fixed by Eq. (16) is given by

$\alpha_S^{(5)}(M_Z)$	0.1161	0.1181	0.1201
\overline{m}_b	4.221 GeV	4.203 GeV	4.184 GeV

Using these masses as inputs and Eq. (15), we can calculate the energy levels of other observed quarkonium states. These are shown in Figs. 3. Only those levels which can be predicted reliably are displayed. The level spacings become wider for larger $\alpha_S^{(5)}(M_Z)$, which is consistent with our naive expectation. If we take an average of the S -wave and P -wave levels corresponding to each principal quantum number n , the theoretical predictions with $\alpha_S^{(5)}(M_Z) = 0.1181$ reproduce the experimental values fairly well. On the other hand, the predictions for the S - P splittings and the fine splittings are smaller than the experimental values.

Also the numerical values of the series expansions of the energy levels are shown in Tab. 1 in the case $\alpha_S^{(5)}(M_Z) = 0.1181$. In this case, the series expansions for the 1^3S_1 , 1^3P_J , 2^3S_1 , 2^3P_0 and 3^3S_1 bottomonium states converge well. For these states the differences of the theoretical predictions and the experimental data are typically 30–60 MeV. Convergence of the series expansions is poor for the $2P_1$, $2P_2$ and $4S$ states. We consider that the theoretical predictions for these levels are unreliable and marked the corresponding theoretical predictions with sharps (\sharp). The differences $E_X^{exp} - E_X$ are rather large for the states with sharps. Notice that for these states the corresponding $\alpha_S(\mu_X)$ becomes larger than one, indicating a breakdown of

[†] We evolve the coupling and match it to the coupling of the theory with $n_l = 4$ via 4-loop running.

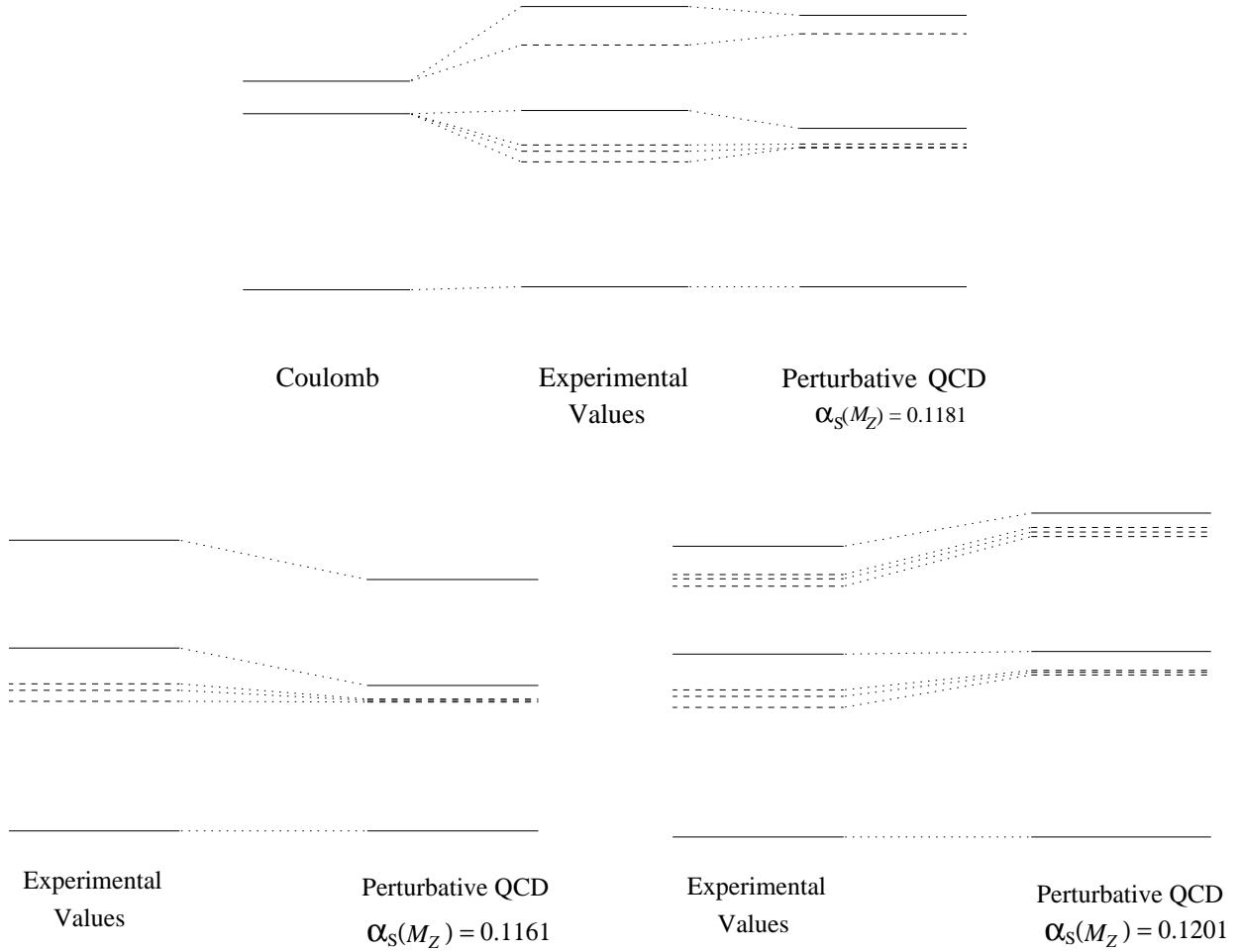


Figure 3: Comparisons of the theoretical predictions and the experimental data for the bottomonium spectrum. The input values of the theoretical predictions are $\alpha_s^{(5)}(M_Z) = 0.1181, 0.1161$ and 0.1201 . We set $m_c = 0$ and the number of massless flavors as $n_l = 4$. The solid and dashed lines represent the S - and P -states, respectively. We show only those levels which we can compute reliably.

State X	E_X^{exp}	E_X	$E_X^{exp} - E_X$	$E_X^{(1)}$	$E_X^{(2)}$	$E_X^{(3)}$	μ_X	$\alpha_S(\mu_X)$
$\Upsilon(1^3S_1)$	9.460	9.460	0	0.837	0.204	0.013	2.49	0.274
$\Upsilon(1^3P_0)$	9.860	9.905	-0.045	1.38	0.115	0.003	1.18	0.409
$\Upsilon(1^3P_1)$	9.893	9.904	-0.011	1.40	0.098	0.002	1.15	0.416
$\Upsilon(1^3P_2)$	9.913	9.916	-0.003	1.42	0.086	0.003	1.13	0.422
$\Upsilon(2^3S_1)$	10.023	9.966	+0.057	1.46	0.093	0.009	1.09	0.433
$\Upsilon(2^3P_0)$	10.232	10.268	-0.036	2.37	-0.66	0.15	0.693	0.691
$\Upsilon(2^3P_1)$	10.255	10.316 [#]	-0.061 [#]	3.97	-3.56	1.50	0.552 [#]	1.20
$\Upsilon(2^3P_2)$	10.268	10.457 [#]	-0.189 [#]	4.55	-5.03	2.53	0.537 [#]	1.39
$\Upsilon(3^3S_1)$	10.355	10.327	+0.028	2.34	-0.583	0.163	0.698	0.684
$\Upsilon(4^3S_1)$	10.580	11.760 [#]	-1.180 [#]	5.45	-6.47	4.38	0.527 [#]	1.61

Table 1: Comparisons of the theoretical predictions of perturbative QCD and the experimental data for $\alpha_S(M_Z) = 0.1181$. All dimensionful numbers are in GeV unit.

the perturbative series. Generally, for states, which we consider reliably calculable, the scale dependence decreases as we include more terms of the perturbative series. For states, whose predictions we consider unreliable, the series becomes much more convergent if we would choose a scale different from (typically larger than) μ_X .

4 Error Estimates

Besides non-perturbative corrections, there are two kinds of uncertainties in our theoretical predictions for the bottomonium spectra. These are listed below and in Tab. 2. Also these examinations indicate that the theoretical predictions for the 2^3P_1 , 2^3P_2 and 4^3S_1 bottomonium states are quite unstable, while the prediction for the 2^3P_0 state is at the boundary.

- 1) *Charm Mass Effects.* We have also made an analysis of the bottomonium spectrum including finite charm mass effects. We will report the full results in a separate paper [23]. Here we only summarize some of the qualitative features of the effects and include them as a part of the uncertainties of our present analysis. The corrections to the reliable predictions turn out to be positive and to become larger for higher states, ranging up to ~ 200 MeV. Much of the effects, however, can be cancelled by decreasing the input $\alpha_S^{(5)}(M_Z)$ within its present uncertainty.[‡]
- 2) *Uncertainties from Higher-Order Corrections.* We take the maximum value of the following five estimates as an estimate of uncertainties from unknown higher-order corrections for each series expansion: (i) The difference between the theoretical predictions computed

[‡] We note that the sensitivities of the higher levels to a variation of $\alpha_S^{(5)}(M_Z)$ increase by the charm mass effects due to the decoupling of the charm quark.

		Estimates of higher-order corrections						$\mu = 2\mu_X$
		(i)	(ii)	(iii)	(iv)	(v)	$\pm\max$	
$\delta\bar{m}_b$		-2	+1	0	± 7	+5	± 7	+16
δE_X	$\Upsilon(1^3P_0)$	+15	-14	0	± 3		± 15	-53
	$\Upsilon(1^3P_1)$	+22	-8	+7	± 2		± 22	-48
	$\Upsilon(1^3P_2)$	+16	-16	0	± 3		± 16	-54
	$\Upsilon(2^3S_1)$	+18	-19	-1	± 9		± 19	-73
	$\Upsilon(2^3P_0)$	+33	-57	-21	± 150		± 150	-120
	$\Upsilon(2^3P_1)$	-4	+1637 [#]	-66 [#]	$\pm 1500^{\#}$		$\pm 1637^{\#}$	-97
	$\Upsilon(2^3P_2)$	-136	+2136 [#]	-206 [#]	$\pm 2530^{\#}$		$\pm 2530^{\#}$	-229
	$\Upsilon(3^3S_1)$	+37	-63	-36	± 163		± 163	-161
$\Upsilon(4^3S_1)$	-639 [#]	+2936 [#]	-1425 [#]	$\pm 4380^{\#}$		$\pm 4380^{\#}$	-1361	

Table 2: Variations of the theoretical predictions of Tab. 1 when the uncertainties 2) discussed in Sec. 4 are separately taken into account. All dimensionful numbers are in MeV unit. Those values corresponding to the unreliable theoretical predictions are marked with sharps. The input parameter is taken as $\alpha_S(M_Z) = 0.1181$. The column “ $\pm\max$ ” lists $\pm\max\{ |(i)|, |(ii)|, |(iii)|, |(iv)|, |(v)| \}$. In the last column we write conservative estimates with the scale choice $\mu = 2\mu_X$.

using $\alpha_S(\mu)$ as obtained by solving the renormalization-group equation perturbatively at 4 loops (Eqs. (3) and (11) of Ref. [24]) and numerically at 4 loops (the data of Tab. 1). (Note that the number of energy levels that can be determined in a reliable way is larger with the former definition of the running coupling constant. Also in that case, reliable predictions turn out to be close to the experimental values.) (ii) The difference between the theoretical predictions computed using the 3-loop and the 4-loop (as in Tab. 1) running coupling constants, fixing $\alpha_S^{(5)}(M_Z) = 0.1181$. (iii) The difference between the theoretical estimates obtained by fixing μ_X on the minimum of $|E^{(3)}|$ and the results of Tab. 1, obtained by fixing μ_X via the condition (15). (iv) The contribution $\pm|E_X^{(3)}|$ from Tab. 1. (v) For the $1S$ states we consider the $\mathcal{O}(\alpha_S^5 m)$ corrections calculated in the large- β_0 approximation in [11].

For comparison, we list more conservative error estimates. These are the variations of \bar{m}_b and E_X when we fix the scale as twice[§] of the minimal sensitivity scale: $\mu = 2\mu_X$, where μ_X is determined from Eq. (15).

[§] If we fix the scale as half of the minimal sensitivity scale, $\mu = \mu_X/2$, the predictions for the $n = 2$ bottomonium states appear to be meaningless, since the scales are quite close to the infrared singularity of the running coupling constant, and the predictions for the $n \geq 3$ states do not exist, since the scales lie below the infrared singularity.

5 Interpretation

The most non-trivial feature of the present theoretical predictions for the bottomonium spectrum is that the level spacings between consecutive n 's are almost constant, whereas in the Coulomb spectrum the level spacings decrease as $1/n^2$. Conventionally, this same difference between the Coulomb spectrum and the observed quarkonium spectra motivated people to construct various potential models. It is, therefore, imperative to elucidate how the above perturbative QCD calculation is able to reproduce such a level structure. We will focus on two points: (1) the leading renormalon cancellation, which implies that infrared physics decouples; this is essential to obtain convergent series expansions; (2) the meaning of the scale μ_X chosen by the scale-fixing prescription (15).

According to the discussion in Sec. 2.2, physical meaning of the renormalon cancellation can be understood as the decoupling of infrared gluons in the computation of the quarkonium energy levels: The gluons, whose wavelengths are much larger than the size of the color-singlet boundstate, cannot couple to it. In Eqs. (13) and (14), the integrands essentially cancel each other in the region $q \lesssim 1/r$. We may replace r by the size a_X of a boundstate X in Eqs. (12)–(14) and write

$$E_X \approx 2\bar{m} + \int_{1/a_X \lesssim q < \bar{m}} \frac{d^3\vec{q}}{(2\pi)^3} C_F \frac{4\pi\alpha_S(q)}{q^2}. \quad (17)$$

This expression may be made somewhat more accurate. Let us approximate the energy level as

$$E_X \equiv 2m_{\text{pole}} + E_{\text{bin},X}, \quad (18)$$

$$2m_{\text{pole}} \simeq 2\bar{m} + \int_{q < \bar{m}} \frac{d^3\vec{q}}{(2\pi)^3} C_F \frac{4\pi\alpha_S(q)}{q^2} = 2\bar{m} + \frac{2C_F}{\pi} \int_0^{\bar{m}} dq \alpha_S(q), \quad (19)$$

$$E_{\text{bin},X} \simeq \langle X | \frac{\vec{p}^2}{m_{\text{pole}}} + V_{\text{QCD}} | X \rangle. \quad (20)$$

Here, $V_{\text{QCD}}(q) \simeq -C_F 4\pi\alpha_S(q)/q^2$ is the QCD static potential in momentum space; $|X\rangle$ denotes the Coulomb wave function (the zeroth-order approximation). From Eqs. (19) and (20) we obtain

$$E_X \simeq 2\bar{m} + \frac{2C_F}{\pi} \int_0^{\infty} dq \alpha_S(q) f_X(q) + \langle X | \frac{\vec{p}^2}{m_{\text{pole}}} | X \rangle \quad (21)$$

$$\simeq 2\bar{m} + \frac{2C_F}{\pi} \int_0^{\infty} dq \alpha_S(q) f_X(q). \quad (22)$$

The last approximation follows from the fact that the kinetic energy contribution to the bottomonium levels turns out to be numerically small* (notice that this does not contradict the

*It is about 17% of $E_X^{(1)}$ for the $X = 1S$ state, 6% of $E_X^{(1)}$ for the $X = 2S$ state, 4% of $E_X^{(1)}$ for the $X = 3S$ state. Moreover, these contributions tend to cancel each other in the level spacings.

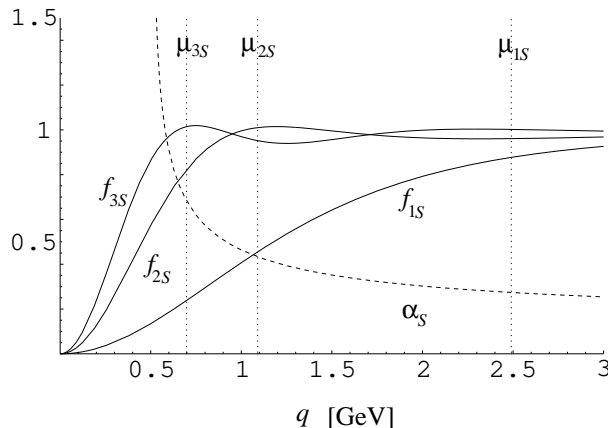


Figure 4: The support functions $f_X(q)$ vs. q for $X = 1S, 2S$ and $3S$ (solid lines). $f_X(q)$ is calculated using $m_{\text{pole}} = 5$ GeV and a different $\alpha_S(\mu_X)$, taken from Tab. 1, for each X . Vertical lines represent the corresponding scales μ_X taken from the same table. Also $\alpha_S^{(4)}(q)$ is shown by a dashed line.

virial theorem, since the static potential we are considering here incorporates the running of α_S and therefore is not simply of the form $1/r$). The support function f_X is given by

$$f_X(q) = \theta(\overline{m} - q) - \int_0^\infty dr r^2 |R_X(r)|^2 \frac{\sin(qr)}{qr}, \quad (23)$$

where $R_X(r)$ is the radial part of the Coulomb wave-function of X . $f_X(q)$ is almost unity in the region $1/a_X \lesssim q < \overline{m}$, where a_X is the inverse of the dumping scale of f_X and may be interpreted as the size of the boundstate X . Thus, Eq. (22) can be identified with Eq. (17) qualitatively.

For the $1S$ state $f_X(q)$ dumps slowly as q decreases. For other states $f_X(q)$ dumps rapidly from scales which are somewhat smaller than the naive expectations $(C_F \alpha_S m_{\text{pole}})/n_X$. In Fig. 4 we show f_X for different states calculated with $m_{\text{pole}} = 5$ GeV and $\alpha_S(\mu_X)$ taken from Tab. 1. The corresponding values of μ_X are also displayed. For those states which we consider the predictions reliable, μ_X is located within the range where $f_X(q) \simeq 1$ (close to the infrared edge); for those states with unreliable predictions, μ_X is located out of this range but far in the infrared region. This comparison shows a relation between the scale μ_X and the wave function (consequently the size) of the corresponding boundstate X .

Eq. (17) or (22) tells that *the major contribution to the energy levels comes from the region $1/a_X \lesssim q \lesssim \overline{m}$ of the self-energy corrections of quark and antiquark* (apart from the constant contribution $2\overline{m}$). That is, with respect to only the contributions of the gluons inside the boundstate, the self-energies of quark and antiquark dominate over the potential energy between the two particles. Hence, we find a qualitative picture on the composition of the energy of a bottomonium state:

- (I) The energy levels of bottomonium are mainly determined by (i) the $\overline{\text{MS}}$ masses of b and \bar{b} , and (ii) contributions to the self-energies of b and \bar{b} from gluons with wavelengths

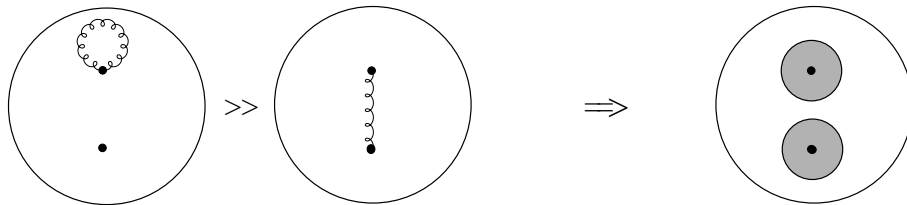


Figure 5: The total energy of a heavy quarkonium state is carried by the $\overline{\text{MS}}$ masses of quark and antiquark and by the gluons inside the boundstate. In the latter contributions the self-energies of quark and antiquark dominate over the potential energy between the two particles.

$1/\overline{m} \lesssim \lambda \lesssim a_X$. The latter contributions may be regarded as the difference between the (state-dependent) constituent quark masses and the current quark masses.

This picture is reminiscent of the (long-established) interpretation that the masses of light hadrons consist of the constituent quark masses. See Fig. 5.

Now we are in a position to see why the level spacings among the bottomonium excited states are much wider than those of the Coulomb spectrum. We know that if the coupling $\alpha_S(q)$ were independent of q , the energy spectrum would become the Coulomb spectrum. In Fig. 4 also $\alpha_S(q)$ is shown. We see that as n_X increases from 1 to 3, the coupling $\alpha_S(q)$, close to the dumping scale of $f_X(q)$, grows rapidly. According to Eq. (17) or (22), as the integral region extends down to smaller q , the self-energy contributions grow rapidly in comparison to the non-running case. They push up the energy levels of the excited states considerably and widen the level spacings among the excited states. Thus, we may draw the following qualitative picture of the bottomonium level structure:

- (II) Level spacing between consecutive n 's increases rapidly with n as compared to the Coulomb spectra. This is because the self-energy contributions (from $1/\overline{m} \lesssim \lambda \lesssim a_X$) grow rapidly as the physical size a_X of the boundstate increases.

6 A Link to Phenomenological Potentials

We return to the problem which we discussed in the introduction (Sec. 1): How can we understand the “linear potential” in the difference between the Coulomb potential and a typical phenomenological potential?

According to the interpretation given in the previous section, the total energy $E_{\text{tot}}(r) \equiv 2m_{\text{pole}} + V_{\text{QCD}}(r)$ of a $b\bar{b}$ system determines the bulk of the bottomonium spectrum. Hence, we examine the series expansion in $\alpha_S(\mu)$ of the total energy, expressed in terms of the b -quark $\overline{\text{MS}}$ mass, $E_{\text{tot}}(r; \overline{m}_b, \alpha_S(\mu))$, and compare it with phenomenological potentials [2]. The obtained total energy depends on the scale μ due to truncation of the series at $\mathcal{O}(\alpha_S^3)$. One finds that, when r is small, the series converges better and the value of $E_{\text{tot}}(r)$ is less μ -dependent if we choose a large scale for μ , whereas when r is larger, the series converges better and the value of

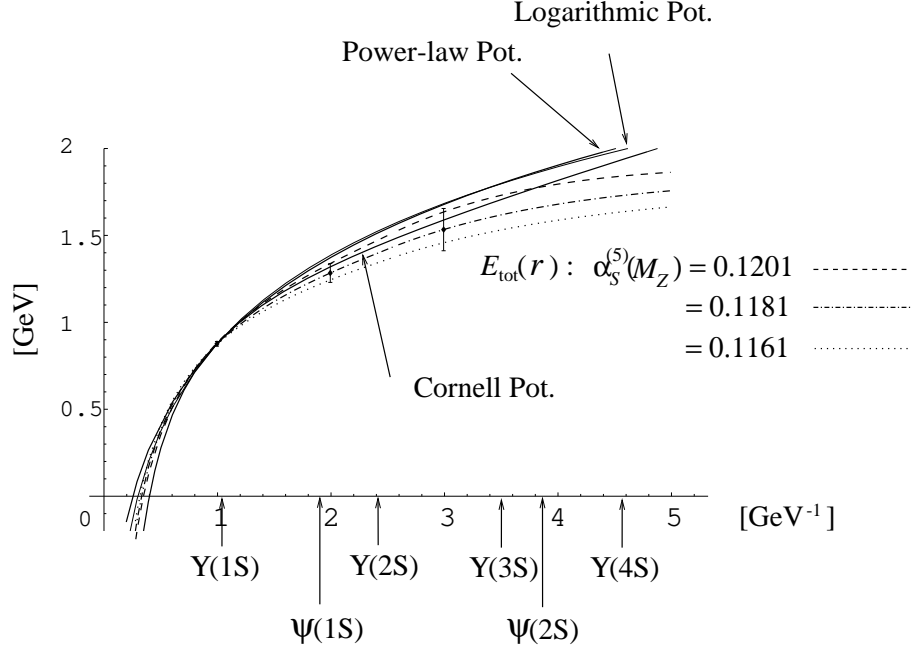


Figure 6: A comparison of the total energy of a $b\bar{b}$ system and typical phenomenological potentials (solid lines). Effects of the non-zero charm quark mass are included. For a reference, we show typical sizes of the bottomonium and charmonium S states as determined from the r.m.s. interquark distances with respect to the Cornell potential: $\sqrt{\langle r^2 \rangle}_{\text{Cornell}}$.

$E_{\text{tot}}(r)$ is less μ -dependent if we choose a smaller scale for μ . Taking into account this property, we will fix the scale μ in two different ways below:

1. We fix the scale $\mu = \mu_1(r)$ by demanding stability against variation of the scale:

$$\mu \frac{d}{d\mu} E_{\text{tot}}(r; \bar{m}, \alpha_S(\mu)) \Big|_{\mu=\mu_1(r)} = 0. \quad (24)$$

2. We fix the scale $\mu = \mu_2(r)$ on the minimum of the absolute value of the last known term [$\mathcal{O}(\alpha_S^3)$ term] of $E_{\text{tot}}(r)$:

$$\mu \frac{d}{d\mu} [E_{\text{tot}}^{(3)}(r; \bar{m}, \alpha_S(\mu))]^2 \Big|_{\mu=\mu_2(r)} = 0. \quad (25)$$

It turns out that the total energy hardly changes whether we choose $\mu = \mu_1(r)$ or $\mu = \mu_2(r)$; also the scales $\mu_1(r)$ and $\mu_2(r)$ are considerably larger than $1/r$; the perturbative prediction for $E_{\text{tot}}(r)$ becomes unstable at $r \gtrsim 3 \text{ GeV}^{-1}$.

In Fig. 6 we compare the total energy for $\alpha_S^{(5)}(M_Z) = 0.1201, 0.1181, 0.1161$ with typical phenomenological potentials:

- A Coulomb-plus-linear potential (Cornell potential) [25]:

$$V(r) = -\frac{\kappa}{r} + \frac{r}{a^2} \quad (26)$$

with $\kappa = 0.52$ and $a = 2.34 \text{ GeV}^{-1}$.

- A power-law potential [26]:

$$V(r) = -8.064 \text{ GeV} + (6.898 \text{ GeV})(r \times 1 \text{ GeV})^{0.1}. \quad (27)$$

- A logarithmic potential [27]:

$$V(r) = -0.6635 \text{ GeV} + (0.733 \text{ GeV}) \log(r \times 1 \text{ GeV}). \quad (28)$$

In order to make a clear comparison, arbitrary constants have been added to all the potentials and $E_{\text{tot}}(r)$ such that their values coincide at $r = 1 \text{ GeV}^{-1}$. The total energy appears to be in good agreement with the phenomenological potentials in the range $0.5 \text{ GeV}^{-1} \lesssim r \lesssim 3 \text{ GeV}^{-1}$. The level of agreement is consistent with the uncertainties expected from the next-to-leading renormalon contributions $[\pm \frac{1}{2} \Lambda_{\text{QCD}} \cdot (\Lambda_{\text{QCD}} r)^2]$ taking $\Lambda_{\text{QCD}} = 300 \text{ MeV}$: indicated by the error bars].

Thus, we confirm that, when the renormalon cancellation is incorporated, the QCD radiative corrections bend the Coulomb potential upwards at long distances. One may understand it similarly to the previous discussion: When the infrared cutoff $\sim 1/r$ of Eqs. (12)–(14) is lowered, i.e. at large r , $\alpha_S(q)$ grows rapidly in the integrand, which raises the total energy as compared to the non-running (Coulomb) case.

Another way to understand it qualitatively is to consider the interquark force defined by

$$F(r) \equiv -\frac{d}{dr} E_{\text{tot}}(r) = -\frac{d}{dr} V_{\text{QCD}}(r) \quad (29)$$

$$\equiv -C_F \frac{\alpha_F(1/r)}{r^2}. \quad (30)$$

The last line defines the “ F -scheme” coupling constant $\alpha_F(\mu)$. The interquark force is also free from the leading renormalon. The running of $\alpha_F(\mu)$ is dictated by the renormalization-group equation:

$$\mu^2 \frac{d}{d\mu^2} \alpha_F(\mu) = \beta_F(\alpha_F), \quad (31)$$

where the first two coefficients of the beta function are universal, i.e. same as those of $\beta_{\overline{\text{MS}}}(\alpha_S)$. When we consider effects of the QCD radiative corrections on the lowest-order Coulomb potential, one may interpret that in the QCD potential, $V_{\text{QCD}}(r) \simeq -C_F \alpha_S(1/r)/r$, the coupling

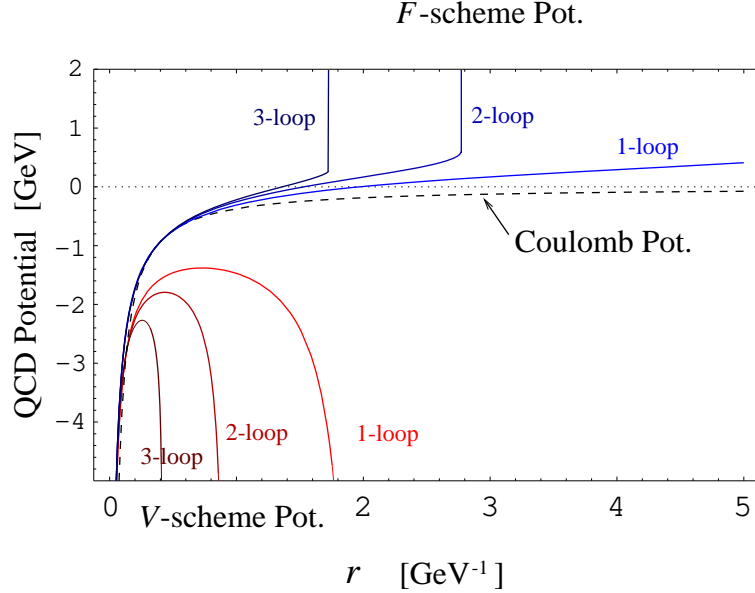


Figure 7: A comparison of the QCD potentials calculated in V -scheme and in F -scheme as well as the Coulomb potential. We set $m_c = 0$ and consider 4 massless flavors. The Coulomb potential is given by $-C_F\alpha/r$ with $\alpha = 0.279$.

increases at long distances, so the potential will be bent downwards. This is a bad interpretation, since the QCD potential is poorly convergent at relevant distances. We should rather consider the interquark force. A better interpretation is that in $F(r) = -C_F\alpha_F(1/r)/r^2$, the F -scheme coupling increases at long distances, and correspondingly $|F(r)|$ grows with respect to the Coulomb force. This means that the slope of the potential becomes steeper at long distances. Its effect resembles an addition of a linearly rising potential to the Coulomb potential. Thus, the effects of the radiative corrections are even qualitatively reversed, whether we consider $V_{\text{QCD}}(r)$ or $F(r)$ as the physically relevant quantity.

One may verify these features in Fig. 7, in which the Coulomb potential, the V -scheme potentials and the F -scheme potentials are displayed. The V -scheme potentials are calculated by solving the renormalization-group equation for the QCD potential. The F -scheme potentials are calculated by first solving the renormalization-group equation (31) for α_F numerically and then by integrating $-F(r)$ over r numerically; arbitrary constants are added such that the F -scheme potentials coincide the Coulomb potential at $r = 0.4 \text{ GeV}^{-1}$. As can be seen, the V -scheme potentials become singular at fairly short distances, whereas the F -scheme potentials have wider ranges of validity. The 2-loop and 3-loop F -scheme potentials are consistent with the phenomenological potentials within the uncertainty expected from the next-to-leading renormalon contributions, in the range $0.5 \text{ GeV}^{-1} \lesssim r \lesssim 2.8 \text{ GeV}^{-1}$ and $0.5 \text{ GeV}^{-1} \lesssim r \lesssim 1.7 \text{ GeV}^{-1}$, respectively. On the other hand, the 1-loop F -scheme potential

does not satisfy this criterion.

7 Conclusions and Discussion

For all the bottomonium states, where the predictions of perturbative QCD can be made reliably (i.e. $\alpha_S < 1$), our results are consistent with the experimental data within the estimated uncertainties of the theoretical predictions. The obtained value for \overline{m}_b is in good agreement with the recent sum-rule calculations. The theoretical uncertainties given in Tab. 2 are numerically of the same size as $\Lambda_{\text{QCD}} \times (a_X \Lambda_{\text{QCD}})^2$, i.e. of the effect of the next-to-leading renormalons: if we approximate $1/a_X \simeq \mu_X$, take the values of Tab. 1, and $\Lambda_{\text{QCD}} = 300 - 500$ MeV, we obtain for the $1S$ state a contribution of order $\pm(5 - 20)$ MeV, for the $n = 2$ states a contribution of order $\pm(20 - 110)$ MeV and for the $3S$ state a contribution of order $\pm(50 - 250)$ MeV. Since the mass \overline{m}_b has been fixed on the vector ground state and has *not* been adjusted for higher states, the data at our disposal suggest that: 1) the bulk of the bottomonium spectrum is accessible by perturbative QCD up to some of the $n = 3$ states; 2) non-perturbative contributions do not need to be larger than 250 MeV for the reliable $n = 3$ states, than 100 MeV for the $n = 2$ states and than 10 MeV for \overline{m}_b , and they are consistent with the type associated with the next-to-leading renormalon. These upper bounds to the non-perturbative corrections are conservative and their true sizes may be considerably smaller; note that for reliable predictions all of $|E_X^{exp} - E_X|$ in Tab. 1 are smaller than 60 MeV.

When we incorporate the cancellation of the leading renormalon contributions, the perturbative expansion of the total energy $E_{\text{tot}}(r)$ of a $b\bar{b}$ system, up to $\mathcal{O}(\alpha_S^3)$ and supplemented by the scale-fixing prescription (24) or (25), converges well at $r \lesssim 3 \text{ GeV}^{-1}$. Moreover, it agrees with the phenomenologically determined potentials in the range $0.5 \text{ GeV}^{-1} \lesssim r \lesssim 3 \text{ GeV}^{-1}$ within the uncertainty expected from the next-to-leading renormalon contributions. This establishes a connection between our present approach based on perturbative QCD and the conventional phenomenological potential-model approaches. Eventually we may merge them and further develop understandings of the charmonium and bottomonium systems. For instance, in the perturbative prediction for the bottomonium spectrum, the level splittings between the S -wave and P -wave states as well as the fine splittings among the nP_j states are smaller than the corresponding experimental values. Although the discrepancy is still smaller than the estimated theoretical uncertainties of the predictions, it should certainly be clarified whether they are explained by higher-order perturbative corrections, or, we need specific non-perturbative effects for describing them. On the other hand, the conventional potential-model approaches have been successful also in explaining the S - P splittings and the fine splittings. Hence, we expect that the connection would help to clarify origins of the differences of the present perturbative predictions and the experimental data.

For what concerns the $c\bar{c}$ system, we obtain $\overline{m}_c = 1243 \pm 15 \pm 20 \pm 50$ MeV from the mass of the J/ψ state: the first error is due to the uncertainty in $\alpha_S(M_Z)$, the second error is due to higher-order corrections, and the third error is due to non-perturbative contributions.

We note that this estimate is in good agreement with recent sum-rule calculations. With the present method, however, we cannot make reliable predictions for states higher than the ground state of charmonium, and, therefore, we cannot extrapolate from consistency arguments the size of the non-perturbative corrections. Nevertheless, from the prediction of the η_c mass, we may anticipate non-perturbative contributions of the order of 100 MeV to the $n = 1$ states. Also this figure is consistent with the next-to-leading renormalon effect (20 – 110 MeV). Our prediction for the mass of the $B_c(1^1S_0)$ state is $M_{B_c(1S)} = 6324 \pm 5 \pm 20 \pm 40$ MeV.

We provided a novel picture on the composition of the masses of the bottomonium states. The picture may be contrasted to that of the QED boundstates such as positronium. For this system, the pole masses of a free electron and positron are well-defined. Then the boundstate mass is given by the sum of the pole masses minus the binding energy. For a bottomonium state, we cannot define the pole masses by separating b and \bar{b} an infinite distance.[†] Therefore, the only sensible description is through contributions of the gluons which reside inside the boundstate. In this picture: the mass of the boundstate becomes heavier than the sum of the quark $\overline{\text{MS}}$ masses (\approx current quark masses); it is composed of the sum of the $\overline{\text{MS}}$ masses and the self-energies (\approx constituent quark masses), supplemented by the small negative potential energy which binds the system together. It would be an interesting question if this picture is also applicable to lighter QCD boundstates.

Acknowledgements

Most of the results reported here are based on the collaboration with N. Brambilla and A. Vairo. The author is grateful for very fruitful discussions.

References

- [1] N. Brambilla, Y. Sumino and A. Vairo, hep-ph/0101305.
- [2] Y. Sumino, hep-ph/0104259.
- [3] E. Eichten and C. Quigg, Phys. Rev. **D49**, 5845 (1994).
- [4] S. Titard and F. Yndurain, Phys. Rev. **D49**, 6007 (1994); Phys. Rev. **D51**, 6348 (1995).
- [5] A. Pineda and F. Ynduráin, Phys. Rev. **D58**, 094022 (1998); **D61**, 077505 (2000).
- [6] K. Melnikov and A. Yelkhovsky, Phys. Rev. **D59**, 114009 (1999).
- [7] N. Brambilla and A. Vairo, Phys. Rev. **D62**, 094019 (2000).

[†] The linear rise at $r \gtrsim 1 \text{ GeV}^{-1}$ and an instability at $r \gtrsim 3 \text{ GeV}^{-1}$ of the perturbative prediction for $E_{\text{tot}}(r)$ may be taken as indicative signatures of quark confinement, at the best of the state of the art of the perturbative QCD prediction.

- [8] A. Hoang, hep-ph/0008102.
- [9] N. Brambilla, A. Pineda, J. Soto and A. Vairo, Phys. Lett. **B470**, 215 (1999); B. Kniehl and A. Penin, Nucl. Phys. **B563**, 200 (1999); Nucl. Phys. **B577**, 197 (2000).
- [10] D. Eiras and J. Soto, hep-ph/0005066.
- [11] Y. Kiyo and Y. Sumino, hep-ph/0007251.
- [12] A. Hoang, M. Smith, T. Stelzer and S. Willenbrock, Phys. Rev. **D59**, 114014 (1999).
- [13] M. Beneke, Phys. Lett. **B434**, 115 (1998).
- [14] A. Penin and A. Pivovarov, Phys. Lett. **B435**, 413 (1998).
- [15] A. Hoang, Phys. Rev. **D61**, 034005 (2000); M. Beneke and A. Signer, Phys. Lett. **B471**, 233 (1999).
- [16] A. Hoang, et al., Eur. Phys. Jdirect **C3**, 1 (2000).
- [17] K. Hasebe and Y. Sumino, Phys. Rev. **D61**, p.105001 (2000).
- [18] A. Hoang and T. Teubner, Phys. Rev. **D58**, 114023 (1998); K. Melnikov and A. Yelkhovsky, Nucl. Phys. **B528**, 59 (1998).
- [19] U. Aglietti and Z. Ligeti, Phys. Lett. **B364**, 75 (1995).
- [20] M. Beneke and V. Braun, Nucl. Phys. **B426**, 301 (1994); I. Bigi, M. Shifman, N. Uraltsev and A. Vainshtein, Phys. Rev. **D50**, 2234 (1994).
- [21] Y. Sumino, “*Renormalon Cancellation in Heavy Quarkonia and Determination of m_b , m_t* ”, hep-ph/0004087.
- [22] D. E. Groom et al., Eur. Phys. Jour. **C15**, 1 (2000).
- [23] N. Brambilla, Y. Sumino and A. Vairo, in preparation.
- [24] K. Chetyrkin, B. Kniehl and M. Steinhauser, Phys. Rev. Lett. **79**, 2184 (1997).
- [25] E. Eichten, K. Gottfried, T. Kinoshita, K. Lane and T. Yan, Phys. Rev. **D17**, 3090 (1978); **D21**, 313(E) (1980); **D21**, 203 (1980).
- [26] A. Martin, Phys. Lett. **93B**, 338 (1980).
- [27] C. Quigg and J. Rosner, Phys. Lett. **71B**, 153 (1977).